geosciences

MDPI

Article

A theory of abrupt climate changes: their genesis and anatomy

Hsien-Wang Ou

Lamont-Doherty Earth Observatory, Columbia University, Palisades, NY10964, USA; hsienou0905@gmail.com

Abstract: We combine our previous ice-sheet and climate models to address abrupt climate changes pertaining to Heinrich (H) and Dansgaard-Oeschger (DO) cycles as well as last deglaciation punctuated by Younger Dryas (YD). We posit their common origin in the calving of the ice sheet but differentiate thermal triggers by geothermal-heat/surface-melt in calving inland/marginal ice, the respective sources of H/DO-cycles. The thermal switches would produce step-like freshwater fluxes to endow abruptness to the resulting climate signals characterized by millennial timescale due to the internal ice dynamics. For an eddying ocean, its response to the freshwater perturbation entails millennial adjustment to maximum entropy production, which would cause sudden post-H warming followed by gradual cooling to form the H-cycles, and the above-freezing warmth (hence surface-melt) would calve the marginal ice to generate DO-cycles anchored on the cooling trend to form the Bond cycle. Since there is already ablation of the Holocene icecap, there would be self-sustained DO-cycles, which thus retain the same pacing as their glacial counterparts to resolve this seeming puzzle. This millennial pacing also transcends the deglaciation to account for its observed sequence although the occurrence of YD requires a boost of the freshwater flux by the rerouted continental meltwater. It is seen that by differentiating thermal triggers of the ice calving and incorporating MEP adjustment of the ocean, the theory has provided an integrated account of the genesis of the abrupt climate changes and their deduced anatomies bear strong resemblance to the observed ones, in support of the theory.

Keywords: abrupt climate change; Heinrich events; Dansgaard-Oeschger cycles; Bond cycles; Younger Dryas; ice-sheet instability; maximum entropy production

Citation: Ou, H.-W. A theory of abrupt climate changes: their genesis and anatomy. *Geosciences* **2022**, *12*, x. https://doi.org/10.3390/xxxxx

Academic Editor: Xianglei Li

Received: date
Accepted: date
Published: date

1. Introduction

Last ice age was teemed with abrupt climate changes pertaining to Heinrich (H) events (HE), Dansgaard-Oeschger (DO) cycles as well as deglaciation punctuated by Younger Dryas (YD), a dramatic climate reversal. While these climate signals are distinct, they are all accompanied by ice-rafted debris (IRD, Bond et al. 1997, Fig. 6), suggesting their common origin in the calving of ice sheet. It is well recognized that large ice sheet is unstable to geothermal heating to periodically calve the inland ice (MacAyeal 1993; Ou 2022), and the anomalous freshwater flux would elicit climate response, as manifested in H-cycles (Bond et al. 1992). Since DO-cycles are associated with much smaller freshwater flux (Yokoyama and Esat 2011), their originating calving must involve only marginal ice (Paillard 1995), but the differentiating physics from that of the inland ice has not been sufficiently articulated, which would be put on a firmer footing in our theory.

Since thermal switch of the ice calving operates on a very short (years) subglacial hydrological timescale (Fricker et al. 2007; Ou 2022), it would generate step-like freshwater flux to endow abruptness to the resulting millennial climate signal. Forgoing such step-like forcing, numerical simulations of H/DO-cycles are sometimes compelled to boost the forcing amplitude to effectuate ocean mode change hence the observed abruptness (Ganopolski and Rahmstorf 2001). And being spanned by ocean modes, both H/DO-cycles would span similar range in the sea surface temperature (SST) with their interstadials being the interglacial --- both departing sharply from the observed cycles whose

interstadials remain well short of the interglacial and the DO-related SST is encased within the H-cycle to form the Bond cycle (Bard 2002, Fig. 2; Elliot et al. 2002, Fig. 3).

That DO-cycles involve ocean mode change is also prompted by large variation in the surface air temperature (SAT) registered in Greenland ice cores (Broecker et al. 1990), which however may simply reflect the extremely cold winter air of the stadials when the ocean heating is blocked by extensive sea ice (Denton et al. 2005; Li et al. 2010). This however should not mask the much-muted variations in SST and meridional overturning circulation (MOC, Elliot et al. 2002; Van Kreveld et al. 2000) --- both negating the interpretation of ocean mode change. Questions have also been raised about calving origin of DO-cycles because of their seeming synchronization among circum-Atlantic ice sheets and the possible lag of IRD to the ocean cooling (Bond and Lotti 1995; Van Kreveld et al. 2000; Barker et al. 2015). Such synchronization however can be facilitated by sea-level coupling (Calov et al. 2002) and the IRD lag can be accounted for by the fast ocean cooling, which would deter melting of icebergs to precede their dislodging of IRD, and then icebergs could be jammed in Denmark Strait and drift slowly with the ocean current as reflected in the spatial thinning of the IRD layer (Van Kreveld et al. 2000; Grousset et al. 1993). In other words, these observations do not necessarily negate possible driving of DO-cycles by the calving of the marginal ice, as we have postulated.

As an alternative to the ocean mode change, DO-cycles have been modelled as self-oscillation of the ocean when it is subjected to hosing or unbalanced initial state (Sakai and Peltier 1999; Brown and Galbraith 2016). The period however is set by the ocean overturning time (Winton and Sarachik 1993), which depends critically on MOC strength hence the anomalous forcing (Sakai and Peltier 1999). It is difficult to reconcile such sensitivity with the similar pacing of the glacial and Holocene DO-cycles (Bond et al. 1997) since MOC is vastly different between the two, and then self-oscillation lacks the observed abruptness (Alley 1998) --- both negating such interpretation.

Instead of a smooth forcing, Menviel et al. (2014) has prescribed step-like freshwater fluxes to examine the climate response, which indeed exhibits abrupt transition between stadials/interstadials (S/IS), and since the modelled temperature range is proportional to the forcing amplitude, it obviously is not set by the ocean modes. This study supports our premise that the thermal trigger of the ice calving together with the fast ocean response are sufficient to produce observed abruptness without invoking ocean mode change. Since the freshwater flux in Menviel et al. (2014) is tuned to produce the observed climate signal, they do not address origin of the forcing, and their modelled interstadials do not exhibit the characteristic cooling, both these shortfalls will be remedied in our theory, which is built upon ice-sheet and climate models previously developed by this author (Ou 2022; Ou 2018). Both these models entail critical but heretofore overlooked physics, as previewed next.

In the ice-sheet model, we shall differentiate thermal switches stemming from the geothermal-heat and surface-melt, which would calve inland/marginal ice in driving the H/DO-cycles, respectively. In addition, the physical closure has removed an entrained empiricism to allow a prognosis of the surge properties, which thus may be justifiably prescribed as external forcing of the ocean. For the climate model, we shall underscore a key process of an eddying ocean stemming from a generalized second law, which would induce salient features of the Bond cycle: the abrupt post-HE warming followed by gradual cooling that anchors DO-cycles. To isolate the governing physics, we seek a *minimal* model which, with lesser latitude for tuning, allows its more critical test against observation. It should be stressed that this minimalistic approach is diametrically opposite to simulation models, which seek *maximal* physics to improve the realism --- often at the expense of understanding and falsifiability. These opposite approaches must be kept in mind when assessing our model simplifications.

For organization of the paper, we shall first discuss the essence of ice-sheet (Section 2) and climate (Section 3) models, which are then applied in sections 4 through 6 to address H/DO-cycles and deglaciation, successively. Within each section, we highlight salient observed features, discuss its genesis and anatomy based on the model physics, and provide synthesis of previous studies for comparison. We conclude the paper in Section 7.

2. Ice-sheet model

Readers are referred to Ou (2022) for a detailed derivation of the ice-sheet model, the following discussion however suffices for self-containment. That a large ice sheet is unstable to geothermal heating to exhibit quasi-periodic surge is first proposed by MacAyeal (1993) and subsequently demonstrated in ice-sheet models (Calov et al. 2002). Physically, ice growth by accumulation would increasingly trap the geothermal heat to warm the bed to the pressure-melting point when a surge is triggered; the ensuing thinning would augment the conductive cooling to refreeze the bed, terminating the surge. As the thermal switch is also favored by greater driving stress, it is sited off the ice divide to calve inland ice discharged through the Hudson Strait, and the ejected icebergs would strew IRD throughout the subpolar water, as seen in the thinning IRD layer following their drift path (Grousset et al. 1993). Numerical simulations of the surge cycle however often involve tuning of the sliding velocity (Calov et al. 2002), which directly impacts its amplitude and period. This empiricism is removed in Ou (2022) by the global momentum balance (Tulaczyk et al. 2000), so the model closure allows us to prognose the surge properties.

A tangible outcome of the model is the construction of a 2-D regime diagram (Fig. 1) spanned by scaled length (l) and width (w) of the ice stream and on which surge properties, such as termination height (h), surge/creep duration (t_s/t_c), and surge velocity (u), can be contoured (all nondimensionalized). It is seen that the model has delineated three dynamical regimes: steady-creep, steady-sliding and cyclic-surge separated by thick and shaded lines, which can be understood as follows. For a short stream, the frictional creep can absorb the accumulation to maintain a steady state, so the thermal switch remains off. For a longer stream, the thermal switch would turn on to trigger the sliding motion whose strength however depends on the strait width: for a narrower strait hence slower sliding, the ice flux can be sustained by catchment to maintain a steady state, but for a wider strait hence faster sliding, the ice flux cannot be sustained, thus vaulting into surge cycles. The box marked H represents ice discharge through the Hudson Strait, which falls well within the surge regime, and the deduced surge properties are comparable with observed ones, including a creep lasting several times the surge, the latter being about a millennium.

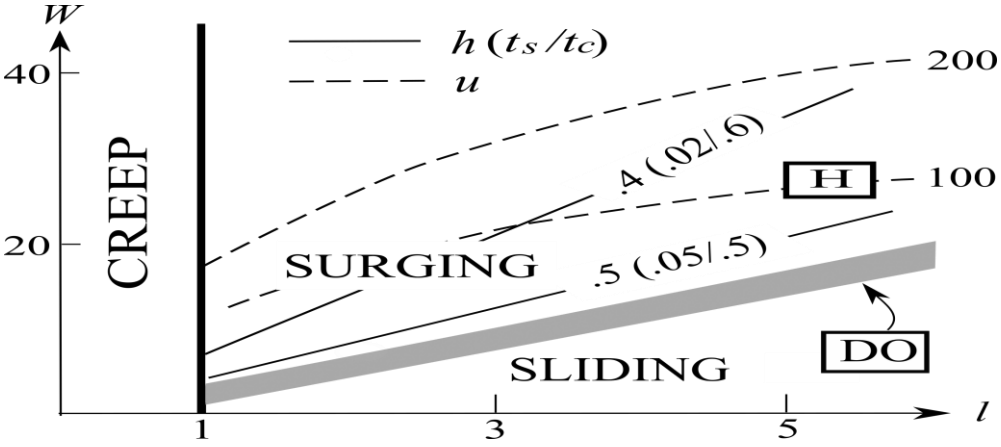

Figure 1. A schematic of the regime diagram spanned by the scaled length l and width w of the ice stream, which consists of steady-creep, steady-sliding and cyclic-surge regimes separated by thick and shaded lines. Contoured surge properties (thin lines) are the termination height (h), surge/creep

duration (t_s/t_c) and surge velocity (u). Box H and shaded line mark the ice discharge for H/DO-cycles, respectively.

Since the DO-cycle has much smaller freshwater flux than the H-cycle, its calving is limited to the marginal ice. Searching for clues that might differentiate the two, we note that englacial ice-sheet temperature shows two distinct zones of temperate bed (Hooke 1977, Fig. 4d): besides the one under ice divide due to the geothermal heat, there is another one in the ablation zone where the surface melt is particularly effective in warming the bed via vertical advection. We posit therefore that the DO-cycle is driven by the thermal switch under the equilibrium line, which would calve the marginal ice of the ablation zone. Unlike ice discharge through the Hudson Strait, this calving may occur along the eastern seaboard of the Laurentide ice sheet (LIS) hence unconstrained by topography, and numerical calculations of ice discharge over a flatbed (Brinkerhoff and Johnson 2015) provide an apt demonstration of its plausible scenario: following the thermal trigger, the surging ice would grow in width until it is arrested by a limit cycle, resulting in periodic self-organized ice streams.

Since the thermal switch underlying Fig. 1 is generic, the stream width arrested by limit cycle is precisely that divides the steady-sliding and cyclic-surge regimes (shaded line). Denoting the corresponding "stream" properties by the subscript "s", they are functions only of the heating parameter defined by the relative strength of the frictional to geothermal heating

$$\alpha_h = \rho_i g \dot{a}[h]/\dot{g} \tag{1}$$

where ρ_i is the ice density, g, the gravitational acceleration, $\dot{a}$, the accumulation, $[h]$, the equilibrium-line altitude (ELA), and $\dot{g}$, the geothermal flux. Specifically, we derive that the termination height is

$$h_s = (\sqrt{1 + 2\alpha_h} - 1)/\alpha_h \tag{2}$$

the aspect ratio of the ice stream is

$$a_s = \sqrt{2}/h_s \tag{3}$$

and the ratio of surge/creep durations is

$$t_{ratio} = 2(1 - a_s^2)^{-1} \tag{4}$$

for which we have set the mean thinning rate during the surge to be half its maximum. They are plotted in Fig. 2 whose qualitative dependence can be explained as follows: for stronger frictional heating, the ice would be thinner before the conductive cooling may terminate the surge, which in turn would be wider on account of the mass balance, and then such wider surge implies faster sliding motion to shorten the surge relative to the creep phases. Applying standard values listed in Appendix, the heating parameter is .48 (dashed), which yields a fractional surface depression of .17, quite smaller than that of the Heinrich events (about .5, see Ou 2022). The surge and creep have comparable duration ($t_{ratio} = 1.1$), both lasting about a millennium. In comparison with the saw-toothed H-cycle, the shorter creep is due to the smaller surface depression during surge, which needs less time to be replenished by accumulation, but the surge duration is maintained by the slower sliding motion hence thinning.

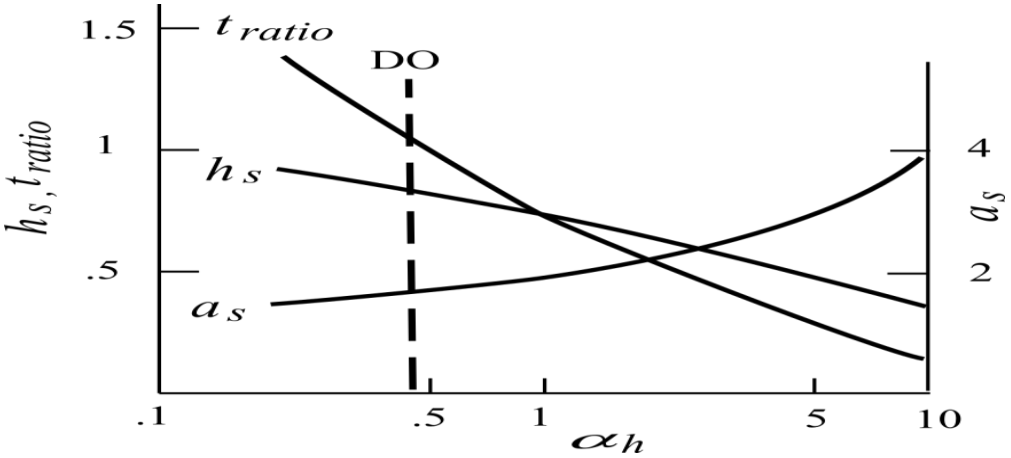

Figure 2. Ice stream properties of the DO-cycle plotted against the heating parameter. They are the termination height h_s, the aspect ratio a_s and the ratio of surge/creep durations t_{ratio}, all nondimensionalized. The vertical dashed line is representative of the DO-cycle, which shows comparable surge/creep durations.

To recap, we have differentiated thermal switches associated with geothermal-heat and surface-melt in calving inland/marginal ice that drive H/DO-cycle, respectively. Because of the physical closure, the deduced surge properties shown in Figs. 1 and 2 are prognostic hence can be prescribed as external forcing of the climate model to be discussed next.

3. Climate Model

Readers are referred to Ou (2018) for detailed derivation of our climate model, and only relevant physics is summarized here for self-containment. The model configuration is sketched in Fig. 3 for which both ocean and atmosphere are composed of warm/cold boxes aligned at mid-latitudes and continental ice sheet would inject anomalous freshwater flux (w) into the subpolar ocean. Since abrupt climate signals are dominated by that of the cold boxes, the model variables are the nondimensionalized cold-box deviations from (known) global-means. The forcing is the deficit in the absorbed SW flux (q), which would differentiate the SST (T) hence SAT via the convective flux (q_c), the resulting atmospheric heat (hence moisture) transport would differentiate the salinity (S), which together with temperature specify the density surplus (ρ), the latter drives MOC (K) across the subtropical front composed partly of random eddy exchange.

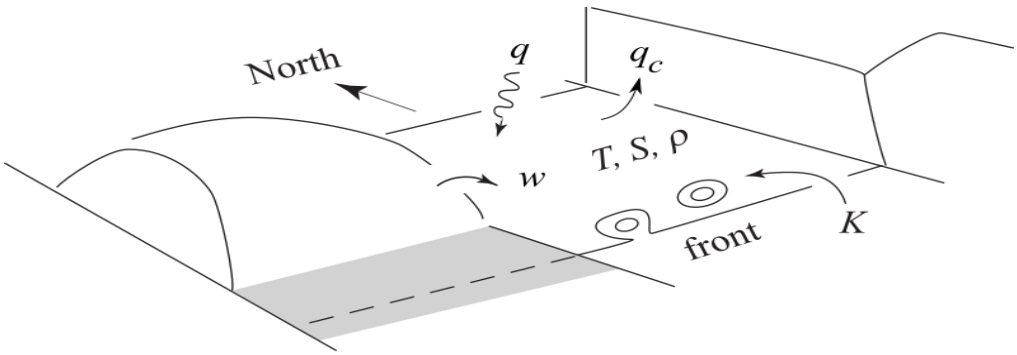

Figure 3. The configuration of a coupled ocean/atmosphere model composed of warm and cold boxes aligned at mid-latitudes and a continental ice sheet injecting anomalous freshwater flux into the subpolar ocean. Model variables are the cold-box deviations from global means and the strength of the MOC (symbols are listed in Appendix).

To illustrate the basic working of our box model, we draw in Fig. 4 the phase-space diagram spanned by MOC and density surplus in which the climate state is specified by

the intersect of two lines: the density curve (thick solid) stemming from thermohaline balance of the ocean, and the "MOC line" (sloping dashed) encoding MOC dependence on the density. Our model, while extremely crude, encapsulates critical but overlooked physics in constraining both these lines, as discussed next.

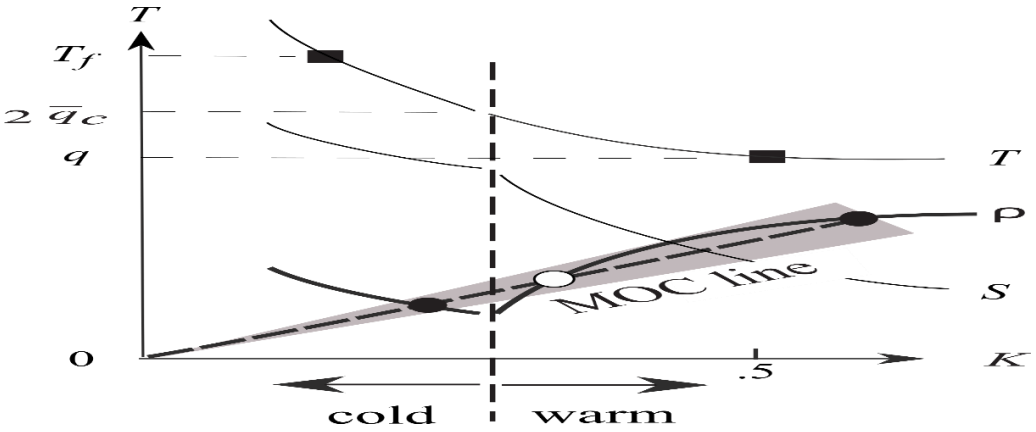

Figure 4. A schematic of the phase-space diagram whereby subpolar temperature/salinity deficit (T/S) and density surplus (ρ) are plotted against MOC (K). The convective bound (vertical dashed) divides warm/cold branches characterized by a slope break in the density curve. The MOC line (sloping dashed) pivots on millennial timescale toward MEP (rectangles), whose intersect with the density curve specifies the climate state (solid ovals). Markings on the ordinate pertain to the temperature.

For the density curve, it represents the difference of temperature and salinity deficits (thin lines, with temperature markings shown on the ordinate). Decreasing MOC would cool and freshen the subpolar water (hence rising deficit lines) accompanied by decreasing convective flux (not shown) hence increasing atmospheric heat transport. The deficit in the convective flux from its global mean ($\bar{q}_c$) is $T/2$ taking into account the concurrent cooling of the surface air, and since the convective flux may not be negative (that is, the deficit may not exceed the global mean), we derive a "convective bound" at

$$T = 2\bar{q}_c \quad (5)$$

marked by the vertical dashed line beyond which (lowering MOC) the convective flux would be nil hence the atmospheric heat transport has saturated at $\bar{q}_c$. As seen from the differing functional dependence of T/S on MOC, the convective bound is characterized by a break in the slope of the density curve, which divides the climate regime into warm/cold branches. In contrast to ocean-only models (Stommel 1961) when the density curve would continue its downward trend to become negative, which has no relevance to the observed ocean, our coupled model allows a normal-signed density contrast through the full range of MOC --- because of the robust convective bound.

Now, about the MOC line, which is straight because of the (assumed) linear dependence of MOC on the density surplus (Stommel 1961; Marotzke and Stone 1995). The proportional constant is coined "admittance" drawing its analogy from the electrostatics with density/MOC playing the role of voltage/current, whose inverse sets the slope of the MOC line. In primitive-equation models that do not resolve eddies, MOC takes the form of a laminar overturning cell, and the admittance is linked to the diapycnal diffusivity, which in effect is a free parameter finely tuned to yield the observed state (Rahmstorf et al. 2005). For the example shown in the figure, the ocean is bistable and the two equilibria (solid ovals, the open oval being the unrealized saddle point) are precisely those discovered by Manabe and Stouffer (1988) and, in support of our convective bound, their cold state is indeed characterized by vanishing convective flux (their Fig. 18).

We attribute the above lack of closure to the inherent turbulent nature of the planetary fluids, so the climate state is a macroscopic manifestation of a nonequilibrium thermodynamics (NT) system, a view increasingly shared among climate theorists (Ou 2001; Ozawa et al. 2003; Kleidon 2009). For a concrete derivation from our box model, we note that admittance is subjected to microscopic fluctuations associated with random eddy exchange across the subtropical front (Auer 1987; Lozier 2010), and applying the fluctuation theorem (FT) --- a generalized second law (Crooks 1999), Ou (2018) deduces that admittance would self-propel on millennial timescale toward maximum entropy production (MEP), a tendency termed "MEP adjustment". Since FT is of considerable mathematical rigor and has been tested in the laboratory (Evans and Searle 2002; Wang et al. 2002), its deductive outcome in MEP further strengthens the latter's physical basis. For visualization, we have blurred the MOC line to symbolize microscopic fluctuations whose probability bias on account of FT would pivot this line toward MEP, the latter as marked by rectangles and discussed next.

For the warm branch, the MEP is derived to be $(T, K = q, 1/2)$, which is consistent with the observed interglacial hence referred as interglacial MEP. For the cold branch, the MEP is given by freezing-point subpolar water $\left(T = T_f\right)$, which nonetheless is free of perennial ice --- the latter is because such ice would cut down the ocean cooling to weaken MOC, in contradiction to MEP. Since adjustment to MEP occurs on millennial timescale, this argument does not preclude sea-ice formation over shorter timescale, such as during HE, as seen later. The deduced cold state is consistent with the observed last glacial maximum (LGM), including its subpolar ocean remaining open in summer (Kucera et al. 2005, Fig. 15; de Vernal et al. 2005, Fig. 10, upper-left panel), which thus will be referred as glacial MEP.

The freshwater flux would displace the density curve, which may be regarded as instantaneous relative to the millennial climate signal. Such displacement would move the climate state from MEP, so the MOC line would then pivot on millennial timescale toward MEP, and our task is simply to discern the climate evolution from the intersect of these two lines, as discussed in the following sections.

4. H-cycle

4.1. Phenomenology

The last glacial was punctuated by recurring Heinrich events (HE) when massive calving of icebergs strewed IRD across the subpolar North Atlantic (Heinrich 1988; Bond et al. 1992; Grousset et al. 1993; Hemming 2004). As discussed in Section 1, the onset and termination of HEs are abrupt relative to their millennial duration (Elliot et al. 2002), and the accompanying freshwater flux is substantial, amounting to a sea-level change of O (10 m) (Chappell 2002), which further depresses the MOC from its already weak glacial strength (Elliot et al. 2002). Since the subpolar water is already at the freezing point (Kucera et al. 2005), a weakening of the MOC causes formation of extensive sea ice (Broecker 1994), which would deter melting of the icebergs as they drift slowly through the subpolar ocean, as seen in the spatial thinning of the IRD layer (Grousset et al. 1993).

The MOC resumes at the termination of HE, but the subpolar water does not just return to the pre-HE state, but an interstadial several degrees warmer (Bard 2002). This post-HE warming is followed by gradual cooling to the pre-HE glacial state, thus exhibiting the saw-toothed H-cycle (Alley 1998; Henry et al. 2016) --- albeit the cooling trend is populated by millennial DO-cycles to form the Bond cycle. While the SAT registered in Greenland ice cores may range over O (10 ^{0}C), the SST variation is considerably smaller with interstadials remaining distinctly cooler than the interglacial (Alley 1998; Bard 2002). The substantial variation in the MOC has led to anti-phased Antarctic climate during abrupt onset of HE, outside of which the hemispheric climates remain synchronous (Broecker 1998; Clark et al. 1999; Stocker 1998).

4.2. Genesis

As discussed in Section 2, our ice-sheet model has produced surge properties comparable with the observed ones, which thus may be prescribed as external forcing of the ocean to examine the resulting H-cycle. Its genesis is illustrated through the phase-space diagram shown in Fig. 5 for which, as a representative example, we have set the annual absorbed SW flux at 90 $W\,m^{-2}$ below the global mean, global convective flux at 56 $W\,m^{-2}$, global-mean SST at 14 ^{0}C and anomalous freshwater flux at .1 Sv (MacAyeal 1993; Menviel et al. 2014) and, given the scales defined in Appendix, they yield dimensionless parameters $(q, \bar{q}_c, T_f, w) = (0.9, 0.56, 1.75, 0.05)$. The corresponding anatomy of the H-cycle is shown in Fig. 6 for which we have set surge/creep duration at 1/5 ky with light/dark shades symbolizing freshwater flux and sea-ice cover, respectively.

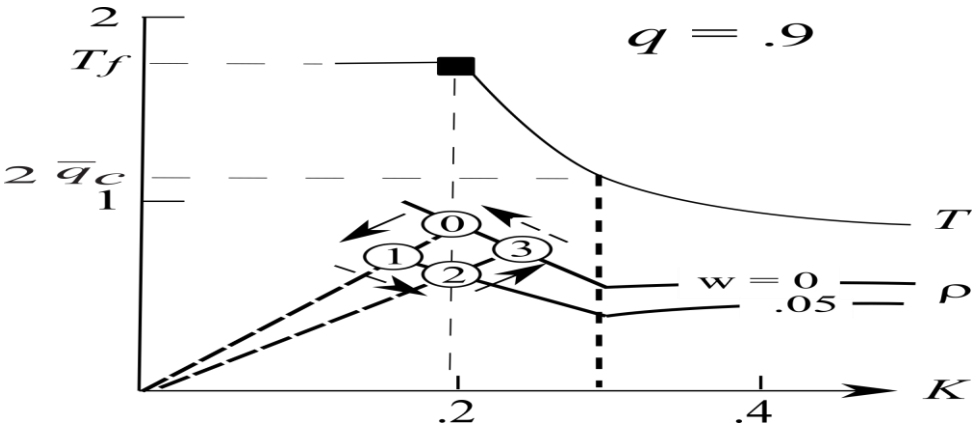

Figure 5. The H-cycle in the phase-space whereby the freshwater flux (w) displaces the density curve (thick solid) and the MOC line (sloping dashed) pivots in response. The cycle goes through numbered states with solid arrows indicating abrupt changes and dashed arrows, the millennial adjustment to MEP (solid rectangle).

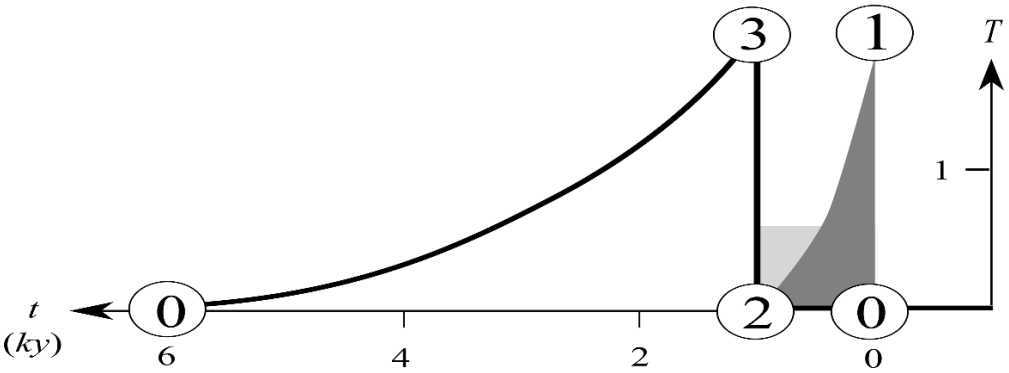

Figure 6. Anatomy (in SST, thick solid line) of the H-cycle corresponding to that of Fig. 5. Light and dark shades symbolize freshwater flux and sea-ice extent, respectively.

The H-cycle begins with the glacial MEP (State 0) when the thermal switch is turned on and runs through numbered states with solid and dashed arrows indicating fast (decadal) and slow (millennial) transits, respectively. Since the MOC line pivots on millennial timescale, it remains immobile at the HE onset, so State 0 would transition to State 1 whereby the weaker MOC would induce extensive sea ice (dark-shaded in the time plot) to maintain the ocean heat balance. During the millennial HE, the MOC line would pivot toward MEP by melting the sea ice to transition State 1 to 2. At the HE termination, the MOC line is again immobile to transition State 2 to 3, which thus exhibits a sudden warming. During the ensuing creep phase, the MEP adjustment would pivot the MOC line toward the glacial MEP (State 0), thus evincing a gradual cooling to form the saw-toothed H-cycle.

A key property of the H-cycle is the post-HE warmth, which can be derived as follows. As the H-cycle resides in the cold branch for which the atmospheric heat transport has saturated at the global-mean convective flux $\bar{q}_c$ (Section 3), the total heat transport (given by the orbital forcing q) is partitioned between atmosphere and ocean as

$$q = \bar{q}_c + KT \quad (6)$$

and the salinity balance states

$$\mu\bar{q}_c + w = KS \quad (7)$$

where μ is the moisture parameter (Ou 2018) so the first term is the atmospheric moisture transport, which together with the freshwater flux w are balanced by the salinity flux carried by the MOC. Combining these two equations yields a density surplus

$$\rho = T - S \quad (8)$$

$$= \frac{1}{K}(q_e - w) \quad (9)$$

where

$$q_e \equiv q - (1+\mu)\bar{q}_c \quad (10)$$

is a property of the unperturbed state. From Eqs. (6), (9) and trigonometry, we derive

$$\frac{T_3}{T_2} = \frac{K_2}{K_3} \quad (11)$$

$$= \frac{\rho_2}{\rho_3} \quad (12)$$

$$= \frac{K_3}{K_2} \cdot \frac{q_e - w}{q_e} \quad (13)$$

so Eqs. (11) and (13) yield

$$\frac{K_2}{K_3} = (1 - \frac{w}{q_e})^{1/2} \quad (14)$$

Substituting Eqs. (14) into (11), we arrive at

$$\frac{T_3}{T_2} = (1 - \frac{w}{q_e})^{1/2} \quad (15)$$

The (dimensional) temperature range (ΔT) of the H-cycle thus is

$$\Delta T = [T](T_2 - T_3)$$

$$\approx \overline{T} \cdot \frac{w}{2\, q_e} \quad (16)$$

for which we have assumed $w/q_e \ll 1$. For parameter values specified earlier, $q_e = .17$, so $w/q_e = .29$, the approximation Eq. (16) thus yields $\Delta T \approx 2\,^0$C, as shown in Fig. 6. Since this warmth increases with the freshwater flux and summer insolation (decreasing q hence q_e), it would lead to deglaciation when certain threshold is exceeded, a topic to be discussed in Section 6.

4.3. Synthesis

The post-HE warmth has been attributed to resumption of the MOC, which however remains short of the interglacial envisioned for the ocean mode change (Paillard 1995; Ganopolski and Rahmstorf 2001). And then the subsequent cooling has been ascribed to the downwind effect of a growing LIS during the binge phase (Alley 1998), whose efficacy remains to be demonstrated (Clark 1992). In our interpretation, both these features are direct consequences of the MEP adjustment: by melting the sea ice during HE, it slightly flattens the MOC line, which necessarily yields a warmer state at the HE termination; then the same process would cool the subpolar water toward the glacial MEP defined by the freezing point; there is no need to invoke disparate physics.

With the gradual cooling being the climate response to HE, it does not precondition HE (Alley and Clark 1999), which runs on the internal ice clock (Section 2). On the other hand, the primary ice calving through the Hudson Strait could synchronize ice calving from other circum-Atlantic ice sheets to augment the freshwater flux (Grousset et al. 1993; Bond and Lotti 1995; Calov et al. 2002). The sea-ice cover during HE is induced by the MOC weakened by freshening, which moreover is dissipating through HE, so a distinct and stable H-mode (Alley and Clark 1999; Rahmstorf 2002) cannot be defined; then the H-cycle spans a temperature range that is proportional to the freshwater flux, as seen in (16) and supported by numerical calculation (Menviel et al. 2014), which further negates its interpretation as ocean mode change. While short of a mode change, the abrupt MOC variation associated with HE is nonetheless of sufficient magnitude to induce anti-phased Antarctic climate (Broecker 1998; Clark et al. 1999; Stocker 2000), outside of which however, the hemispheric climates remain synchronized by global teleconnection (Broecker 1998).

To recap, the interplay between step-like freshwater flux and millennial MEP adjustment has produced a H-cycle consisting of abrupt post-HE warming followed by gradual cooling (Fig. 6), an anatomy that is consistent with observation but not yet properly simulated by numerical models.

5. DO-cycle

5.1. Phenomenology

The cooling phase of the H-cycle is populated by DO-cycles to form the bundled Bond cycle (Dansgaard et al. 1993; Bond et al. 1993). Its hierarchical structure is intriguing: DO-cycles emerge only after post-HE warming and their interstadials track the H-cooling trend. The stadials are accompanied by IRD (Bond et al. 1997; van Kreveld et al. 2000), just like HE, but the freshwater flux is quite smaller (Yokoyama and Esat 2011), suggesting calving of the marginal ice. Its SAT range is large, being of O (10 ^{0}C), which is attributable to the extremely cold winter-air during stadials, but its SST variation is further muted from that of the H-cycle (Bond et al. 1997; Elliot et al. 2002). DO-correlated MOC cannot be discerned nor can the bipolar climate seesaw (Elliot et al. 2002; Charles et al. 1996). Unlike saw-toothed H-cycles, DO-cycles are more symmetric with comparable millennial durations of S/IS (Alley 1998).

Perhaps the most significant observation of DO-cycles is their prevalence in Holocene (Bond et al. 1997; Schulz and Paul 2002), which share common features with their glacial counterpart: they are accompanied by IRD of similar concentration and pacing; and the climate shift are abrupt occurring over centennial timescale (Bond et al. 1997; Grootes and Stuiver 1997). On the other hand, without the sea ice covering the subpolar water during the Holocene, the SAT signal is much reduced and, together with small SST and MOC variations, they represent merely perturbation of the interglacial climate, not ocean mode change.

5.2. Genesis

We have posited in Section 2 that DO-cycles have their origin in the quasi-periodic calving of the marginal ice in the ablation zone. Since during the glacial time, there can be ablation only by the post-HE warming, the glacial DO-cycles are preconditioned on HE and anchored on the cooling phase of the H-cycle to form the Bond cycle. The genesis of DO-cycles is illustrated in the phase space in Fig. 7, which is encased within the H-cycle marked by the thin outer line. Following the same convention as the H-cycle, DO-cycles go through numbered states with solid and dashed arrows indicating fast (centennial) ocean response and slow (millennial) MEP adjustment, respectively, and the corresponding anatomy is plotted in Fig. 8 for which we have applied square-wave freshwater flux of 2 ky period (shaded columns, Bond et al. 1999, Fig. 8) and dark shades symbolize the sea-ice cover.

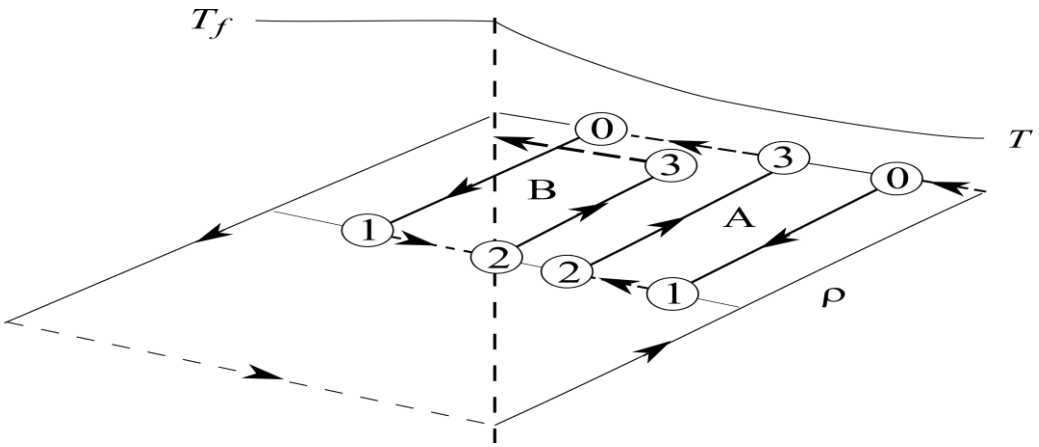

Figure 7. Same as Fig. 5, but for DO-cycles encased within the H-cycle (thin outer lines). Type-A's stadials remain above the freezing point while type-B's stadials have reached the freezing point to resemble a mini-H-cycle.

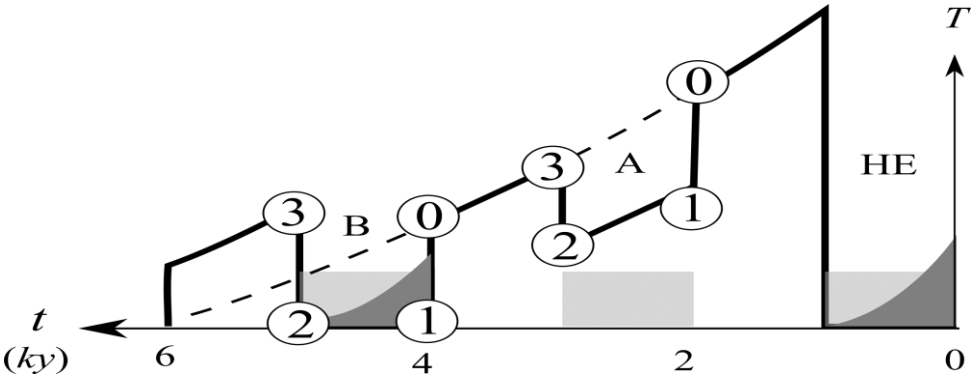

Figure 8. Anatomy (in SST) of DO-cycles corresponding to that shown in Fig. 7 when the freshwater flux is a square-wave of 2 ky period (light shades). Type B's stadial has reached freezing-point to cause formation of the sea-ice (dark shades), resulting in a greater rebound of the ensuing interstadial, but otherwise both S/IS trend as the H-cooling curve (dashed) to exhibit the hierarchical Bond cycle.

Unlike the H-cycle, we need to distinguish two types of DO cycles, designated as type-A and B. For type-A, its stadial remains above the freezing point hence unobstructed in its trending of the H-cooling, so the ensuing interstadial simply returns to the H-cooling curve in the time plot. For type-B however, its stadial has reached the freezing point to cause formation of the sea ice, just like the H-cycle depicted in Figs. 5 and 6, so the ensuing interstadial would protrude above the cooling curve, resembling a miniature post-H warming. This type-B DO-cycle is arguably discernible in observations (see Bond et al. 1993, Fig. 2 between H4 and H3). Despite the protrusion, both S/IS trend as H-cooling to exhibit hierarchical Bond cycle, as depicted in Alley (1998, Fig. 1).

While time signature of DO-cycles is controlled by internal ice dynamics, their initial trigger is due to the post-HE warmth, whose timing thus is related to vertical advection associated with the surface melt. As a cursory estimate, a summer melt rate of 2 $m\,y^{-1}$ (Oerlemans 1991) would yield vertical- and annual-averaged vertical velocity of O (0.5 $m\,y^{-1}$) to render an advective timescale of O (1 ky) hence it need not be differentiated from S/IS durations. With the thermal switch pinned by the post-HE warmth, calving of the marginal ice from circum-Atlantic ice sheets would be synchronized, the latter is also boosted by the marginal ice being more susceptible to sea-level or climate perturbation in resolving this seeming puzzle (Bond et al. 1997).

5.3. Synthesis

Since DO-cycles are accompanied by IRD (Bond et al. 1997), we posit that they are originated in the ice-sheet instability, just like HE, except the thermal switch lies under the ablation zone to calve the marginal ice. This origin avails DO-cycles with step-like freshwater flux of millennial duration --- their defining characteristics in common with the H-cycle; but differing from the latter, glacial DO-cycles commence only after the post-HE warmth has set up the ablation zone to activate their thermal switch, the reason that glacial DO-cycles are encased within the H-cycle to form the hierarchical Bond cycle (Bond et al. 1993). In Holocene, on the other hand, the ablation zone is already in existence around Greenland ice sheet (Oerlemans 1991), so DO-cycles would be self-sustaining and retain the same time signature as their glacial counterparts. This commonality thus stems from ice dynamics of the ablation zone, not the large ice sheet whose absence in Holocene has led Bond et al. (1997) to conjecture an unknown climate forcing, a proposition that is no longer necessary.

As noted in Section 1, above commonality between Holocene and glacial DO-cycles also negates some previous interpretations of the latter, including ocean mode change and self-oscillation. Since Holocene DO-cycles represent only a small perturbations of the interglacial climate, they obviously do not involve ocean mode change; and then the much stronger MOC of the Holocene is what induces the Atlantic multi-decadal variability (Kerr 2000), not the millennial DO-cycles.

To recap, we propose the calving of the marginal ice in the ablation zone as the origin of DO-cycles, which may provide a unified account of the glacial Bond cycles (Fig. 8) and the self-sustaining Holocene DO-cycles, thus removing a significant puzzle of their shared statistics.

6. Deglaciation

6.1. Phenomenology

The most dramatic abrupt changes occurred during last deglaciation, which was preceded by H1 and derailed by a temporary return to deep freeze in YD (Alley and Clark 1999). Multiple freshwater fluxes are identified, which are accompanied by IRD and retain the millennial pacing of DO-cycles (Keigwin et al. 1991, Fig. 6; Bond et al. 1997, Fig. 6), suggesting their origin in the calving of the ice sheet. In addition, there are two massive meltwater pulses (MWP-1A and 1B) derived from melt back of the LIS by the interglacial warmth (Fairbanks 1989).

The meltwater is rerouted from Mississippi to St. Lawrence rivers when LIS has sufficiently retreated, which has augmented the calving-induced freshwater flux to cause YD (Broecker et al. 1988; Teller 1990; Marchitto and Wei, 1995). The coldness of YD however halts MWP-1A as seen in the glacial readvance (Broecker et al. 1988), resulting in only small overlap between the two (Lehman and Keigwin 1992). Since LIS has largely disintegrated during the Preboreal, MWP-1B causes only moderate cooling marking the 8.2 ka event (Alley et al. 1997). As an added puzzle, the YD-like climate reversal did not occur during the penultimate deglaciation (Carlson 2008).

As freshening and cooling have opposite effects on marine $\delta^{18}O$, their relative importance may muddle the interpretation of this data (Keigwin et al. 1991). Both H1 and YD however manifest strongly in the ice-core $\delta^{18}O$ because of the extremely cold winter air (Denton et al. 2005), and the shutdown of MOC during these events has caused Antarctic warming and rising global pCO_2 (Broecker 1998; Shakun et al. 2012), which thus precede the northern climate rebound.

6.2. Genesis

We illustrate the genesis and anatomy of deglaciation in Figs. 9 and 10, respectively. Since the freshwater flux is derived from the same source as that of DO-cycles, it is set as a square wave of 2 ky period (light-shaded), which turns out to reproduce the observed sequence as labelled. We have drawn two meltwater pulses caused by the interglacial warmth based on observations and the timing constraint noted above. Since the summer insolation has risen from the deep glacial, we set $q = .8$ (that is, annul absorbed solar flux is 80 Wm^{-2} below the global mean) so the temperature (deficit) and density (surplus) curves are lowered from those of Fig. 5 and for simplicity we set the same freshwater flux of .1 Sv.

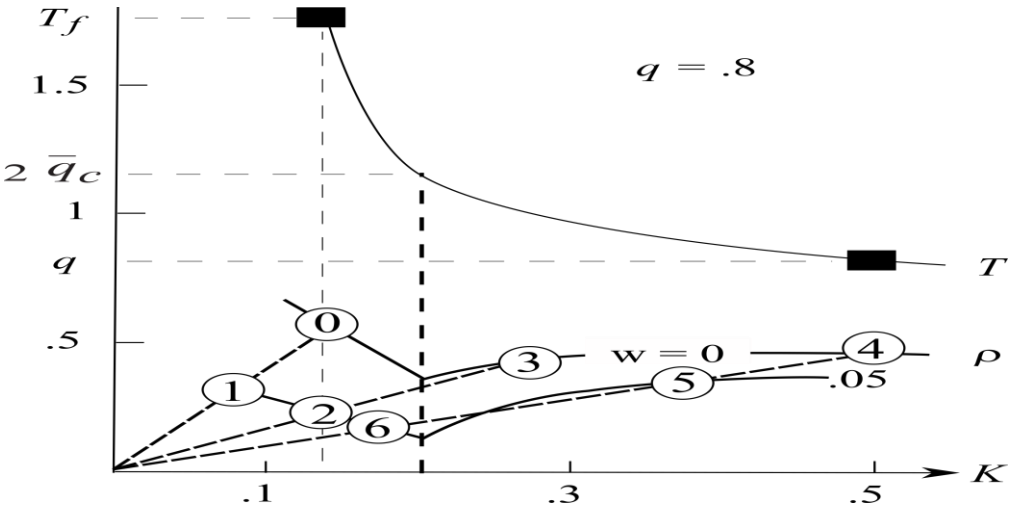

Figure 9. Same as Fig. 5 (arrows neglected for clarity) but for $q = .8$, illustrating genesis of the deglaciation.

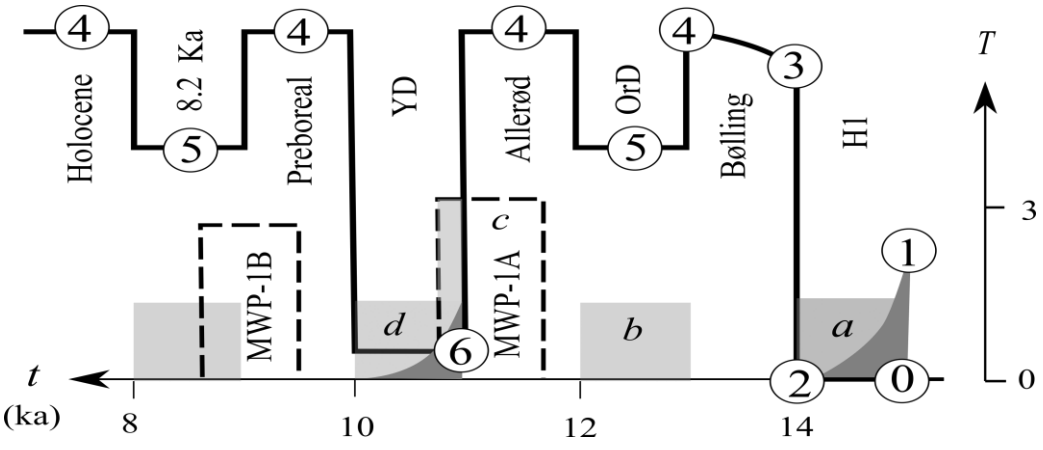

Figure 10. Anatomy of the deglaciation corresponding to that of Fig. 9 with observed events labelled. Light shades are freshwater fluxes of a square wave of 2-ky period with letters *a-d* corresponding to meltwater events identified in Keigwin et al. (1991). Dark shades indicate sea-ice covers.

The climate signal begins with the glacial MEP (State 0) and runs through numbered states. The transition from State 0 to 1 to 2 are like the H-cycle, but because of the rising summer insolation, the MOC line flattened by HE no longer intersects the density curve in the cold branch at the HE termination, so the climate would vault into the warm branch (State 3), marking the initial deglaciation. Equating the post-HE temperature Eq. (15) with the convective bound Eq. (5), we derive a criterion for the deglaciation

$$\frac{w}{q_e} \geq 1 - \left(\frac{2\bar{q}_c}{T_f}\right)^2 \quad (17)$$

The rhs depends on global-mean temperature and convective flux, which set the long-term super-orbital condition; the lhs on the other hand depends on the freshwater perturbation and orbital forcing: a greater freshwater flux would cause deglaciation even with lower summer insolation. With standard parameters listed in Appendix, the rhs is .59; and for meltwater flux of .1 Sv, the deglaciation would occur when annual absorbed SW flux reaches about 81 Wm^{-2} below the global mean, consistent with that seen in Fig. 9. In comparison, the orbital forcing needs to be 8 Wm^{-2} higher without HE; but since such insolation increase is nonetheless attained in about a millennium, HE may not delay the deglaciation (McCabe and Clark 1998) and possibly even hasten it. On the other hand, since recurring time of HE is shorter than half precession cycle (10 ky), it always punctuates the deglaciation, as is the observed case (McManus et at. 1999, Fig. 4).

Following the initial deglaciation, State 3 would propel to State 4 (the interglacial MEP), a transition spanning the Bølling interstadial. The warmth would elevate the snowline to cause calving of the marginal ice after a millennium, just like the DO-cycle, and the resulting freshwater flux would cool State 4 to 5 marking the Older Dryas (OrD), which however remains an interglacial. The continuing Allerød warmth (State 4) would melt back LIS to generate massive MWP-1A, but differing from the northern calving, the meltwater does not perturb the climate until the ice margin has sufficiently retreated to allow its rerouting to the Hudson Bay. And then it would reinforce the northern calving by further lowering the density curve (not drawn) to vault State 4 to 6 marking the YD. Unlike calving paced by internal ice dynamics, the melt back would be halted by the cold YD, as seen in the glacial readvance. Here for simplicity, we have neglected the lesser pivot of the MOC line during YD because the small density surplus has in effect rigidified the MOC line (Ou 2018), so the termination of the millennial YD would rebound the climate from State 6 to 4, the latter corresponding to the Preboreal. The recurring ice calving after a millennium causes the 8.2 ka cooling event (State 5), which is analogous to OrD, and since LIS has largely disintegrated during Preboreal, MWP-1B is insufficient to cause the glacial flip. After the 8.2 ka event, the climate returns to State 4 corresponding to the Holocene.

6.3. Synthesis

The ultimate driver of deglaciation is the rising summer insolation during increasing eccentricity, the suborbital deglaciation events however can be explained by the interplay of three distinct sources of the freshwater perturbation. The first is calving of the inland ice that triggers H1, whose post-event warming would vault the glacial into interglacial. The latter sets up an ablation zone to enable the second source: a quasi-periodic calving of the marginal ice, just like that drives the millennial DO-cycle, whose stadials can be identified with OrD, YD and 8.2 ka event. The glacial flip of YD however requires a third source: the rerouting of the meltwater generated by melt back of LIS (MWP-1A). Since rerouting occurs only after LIS has sufficiently retreated, and the cold YD would halt the melt back, there can only be a small overlap between YD and MWP-1A (Duplessy et al. 1992; Lehman and Keigwin 1992). This timing mismatch has raised question about their causal linkage (Fairbanks 1989), which however is resolved here by the combined effect of second and third freshwater sources. Since YD involves happenstance of rerouting and remnant of the meltwater, such dramatic climate reversal is not inevitable and indeed did not happen during MWP-1B or penultimate deglaciation.

Since YD is characterized by IRD, it has sometimes been designated as H0 (Alley and Clark 1999), which however differs from other HEs in that it is initiated from an interglacial state. As such, YD is accompanied by both strong cooling and freshening, which tend to cancel each other to leave little imprint on the marine δ^{18}O data (Alley and Clark 1999). In contrast, H1 is initiated from the glacial state, so freshening would dominate to register

in this data (Duplessy et al. 1992, Fig. 1). Both YD and H1 however manifest strongly in the ice-core $\delta^{18}O$ because of the extremely cold winter-air insulated from ocean heat by the extensive sea ice (Denton et al. 2005). The first three freshwater fluxes and MWP-1A shown in Fig. 10 can be identified with the four meltwater events discerned in Keigwin et al. (1991, their Fig. 6), and our model offers a plausible interpretation of their puzzling marine $\delta^{18}O$ signature: events *a* and *d* are associated with strong cooling (as symbolized by the shaded sea-ice cover) to cause maxima in the data, but events *b* and *c* involve little cooling hence dominated by freshening to yield minima.

While YD is triggered by freshwater flux, its freshening is due primarily to the MOC shutdown (Duplessy et al. 1992), which would sequester the southern heat to cause Antarctic warming (Broecker 1998; Stocker 2000). As such, the latter and the accompanying rising pCO_2 precede the northern climate rebound (Shakun et al. 2012), which however are not causal since the northern deglaciation is already underway and only temporarily reversed by YD on account of the internal ice dynamics. The termination of YD is accompanied by doubling of accumulation, which has been attributed to atmospheric circulation change (Alley et al. 1993) but it may simply reflect the more moist interglacial air, just like that induced by global warming.

That the enhanced moisture transport by global warming may shut down MOC, like triggering of the YD, is a topic widely discussed in the literature (Manabe and Stouffer 1999; Rahmstorf et al. 2005; Ou 2018). Model intercomparisons however show considerable uncertainty in the bifurcation threshold, which may nonetheless be assessed from our model. As the northern summer insolation has dimmed since about 10 ka (Alley and Clark 1999), it would raise the freshwater threshold based on our phase-space diagram (comparing Figs. 5 and 9), but even the lower threshold and the massive MWP-1B at 8 ka have caused only moderate cooling, we envisage therefore little prospect of a glacial flip; the next glaciation is likely gradual, evolving over millennial timescale, just like previous ones.

To recap, we show that square-wave freshwater flux of 2 ky period, same as that driving the DO-cycles, may reproduce the observed deglaciation sequence (Fig. 10), including YD when such flux is augmented by rerouting of the continental meltwater.

7. Conclusions

We combine our ice-sheet and climate models to address abrupt climate changes pertaining to H/DO-cycles and the last deglaciation punctuated by YD. Since they are all accompanied by IRD, we posit a common origin in the quasi-periodic calving of the ice sheet due to thermal switch at its bed. We distinguish however thermal switches associated with geothermal-heat/surface-melt, which would calve inland/marginal ice to drive H/DO-cycle, respectively. Since the surface-melt requires post-HE warmth during the glacial time, the glacial DO-cycles are encased within the H-cycle to form the hierarchical Bond cycle whereas Holocene DO-cycles are self-sustaining. Otherwise, they should share the same time signature of millennial duration and abruptness, as indeed observed, and there is no need to conjecture unknown climate forcing for such commonality.

In addition to the common forcing by the freshwater flux, we discern a key process in the ocean response, which would propel MOC toward MEP on millennial timescale. Because of this MEP adjustment, there would be sudden post-HE warming followed by gradual cooling, which would anchor DO-cycles to form the Bond cycle, a prominent feature that has not been sufficiently explained previously. For deglaciation, the calving-induced freshwater flux is augmented by rerouting of the continental meltwater to produce climate reversal as seen in YD. It is surprising that a square-wave freshwater flux of 2 ky period prognosed from our ice sheet model is sufficient to reproduce observed anatomy of Bond cycle and deglaciation.

In conclusion, by incorporating calving-induced freshwater flux and MEP adjustment of the ocean, our theory has provided an integrated account of the genesis of abrupt climate changes whose modelled anatomies (Figs. 6, 8 and 10) bear strong resemblance to the observed ones, in support of the theory.

Funding: This research received no external funding.

Data Availability Statement: Not applicable

Conflicts of Interest: This author declares no conflict.

Acknowledgments: None.

Appendix

a_s	Aspect ratio of surging ice
$\dot{a}$	Accumulation (= .1 $m\ a^{-1}$)
$C_{p,o}$	Specific heat of ocean (= 4.2 × $10^3\ J\ Kg^{-1}\ ^0C^{-1}$)
g	Gravitation acceleration (= 9.8 $m\ s^{-2}$)
$\dot{g}$	Geothermal flux (= 6 × $10^{-2}\ Wm^{-2}$)
h_s	Ice height at surge termination
$[h]$	ELA for DO-cycle (= .5 km)
K	MOC mass flux
$[K]$	Scale of K (= $\alpha^* l(2\rho_o C_{p,o})^{-1} = 6\ m^2 s^{-1}$)
l	Latitudinal span of subpolar ocean (= 4 × $10^3\ km$)
L	North Atlantic basin width (= 6 × $10^3\ km$)
q	Cold-box deficit of absorbed solar flux
q_e	Excess forcing over warm-transition threshold
$[q]$	Scale of q (= 100 Wm^{-2})
$\bar{q}_c$	Global convective flux
S	Cold-box salinity deficit
S_0	Reference salinity (=35)
$[S]$	Scale of S (= $\alpha[T]/\beta$=1)
t_{ratio}	ratio of surge/creep duration
$[t]$	Timescale for DO-cycle (≡ $[h]/\dot{a}$ = 5 ky)
T	Cold-box SST deficit
T_c	Convective-bound temperature
T_f	Freezing-point temperature
$[T]$	Scale of T(= $[q]/\alpha^*$ = 8 ^{0}C)
$\bar{T}$	Global-mean SST (=14 ^{0}C)
ΔT	Temperature range of H-cycle
w	Freshwater flux
$[w]$	Scale of w (= $2[K][S]/S_0 = .34\ m^2 s^{-1}$)
α	Thermal expansion coefficient (= $10^{-4}\ ^0C^{-1}$)
α_h	Heating parameter (=.48)
α^*	Air-sea transfer coefficient (= 12.5 $Wm^{-2}\ ^0C^{-1}$, Ou 2018)
β	Saline contraction coefficient (= 8 × 10^{-4})
ρ	Cold-box density surplus
$[\rho]$	Scale of ρ (= $\rho_o \alpha[T] = .8\ Kg\ m^{-3}$)
ρ_i	Ice density (= .92 × $10^3\ Kg\ m^{-3}$)
ρ_o	Reference ocean density (= $10^3\ Kg\ m^{-3}$)
μ	Moisture parameter (= 0.3)

References

Alley RB (1998) Icing the north Atlantic. Nature 392(6674):335-7 https://doi.org/10.1038/32781

Alley RB, Clark PU (1999) The deglaciation of the northern hemisphere: a global perspective. Annu Rev Earth Planet Sci 27(1):149-82 https://doi.org/10.1146/annurev.earth.27.1.149

Alley RB, Mayewski PA, Sowers T, Stuiver M, Taylor KC, Clark PU (1997) Holocene climatic instability: A prominent, widespread event 8200 years ago. Geol 25:483–6 https://doi.org/10.1130/0091-7613(1997)025<0483:hciapw>2.3.co;2

Alley RB, Meese DA, Shuman CA, Gow AJ, Taylor KC, Grootes PM, White JWC, Ram M, Waddington ED, Mayewski PA, Zielinski GA (1993) Abrupt increase in snow accumulation at the end of the Younger Dryas event. Nature 362:527-529 https://doi.org/10.1038/362527a0

Auer SJ (1987) Five-year climatological survey of the Gulf Stream system and its associated rings. J Geophys Res (92):11709–26 https://doi.org/10.1029/jc092ic11p11709

Bard E (2002) Climate shock-Abrupt changes over millenial time scales. Phys Today 55(12):32-8 https://doi.org/10.1063/1.1537910

Barker S, Chen J, Gong X, Jonkers L, Knorr G, Thornalley D (2015) Icebergs not the trigger for North Atlantic cold events. Nature 520(7547):333-6 https://doi.org/10.1038/nature14330

Bond G, Broecker W, Johnsen S, McManus J, Labeyrie L, Jouzel J, Bonani G (1993) Correlations between climate records from North Atlantic sediments and Greenland ice. Nature 365(6442):143-7 https://doi.org/10.1038/365143a0

Bond G, Heinrich H, Broecker W, Labeyrie L, McManus J, Andrews J, Huon S, Jantschik R, Clasen S, Simet C, Tedesco K (1992) Evidence for massive discharges of icebergs into the North Atlantic ocean during the last glacial period. Nature 360(6401):245-9 https://doi.org/10.1038/360245a0

Bond GC, Lotti R (1995) Iceberg discharges into the North Atlantic on millennial time scales during the last glaciation. Science 267(5200):1005-10 https://doi.org/10.1126/science.267.5200.1005

Bond G, Showers W, Cheseby M, Lotti R, Almasi P, DeMenocal P, Priore P, Cullen H, Hajdas I, Bonani G (1997) A pervasive millennial-scale cycle in North Atlantic Holocene and glacial climates. Science 278(5341):1257-66 https://doi.org/10.1126/science.278.5341.1257

Bond GC, Showers W, Elliot M, Evans M, Lotti R, Hajdas I, Bonani G, Johnson S (1999) The North Atlantic's 1-2 kyr climate rhythm: relation to Heinrich events, Dansgaard/Oeschger cycles and the Little Ice Age. In: Clark PU, Webb R, Keigwin L (Eds.) Mechanisms of Millennial-Scale Global Climate Change, Geophys Monogr-AGU 112:35–58

Brinkerhoff DJ, Johnson JV (2015) Dynamics of thermally induced ice streams simulated with a higher-order flow model. J Geophys Res Earth Surf 120(F9):1743–70 https://doi.org/10.1002/2015jf003499

Broecker WS (1994) Massive iceberg discharges as triggers for global climate change. Nature 372:421-4 https://doi.org/10.1038/372421a0

Broecker WS (1998) Paleocean circulation during the last deglaciation: A bipolar seesaw? Paleoceanogr 13:119–21 https://doi.org/10.1029/97pa03707

Broecker WS, Andree M, Wolfli W, Oeschger H, Bonani G, Kennett J, Peteet D (1988) The chronology of the last deglaciation: Implications to the cause of the Younger Dryas event. Paleoceanogr Paleoclimatol 3(1):1-9 https://doi.org/10.1029/pa003i001p00001

Broecker WS, Bond G, Klas M, Bonani G, Wolfli W (1990) A salt oscillator in the glacial Atlantic? 1. The concept. Paleoceanogr 5(4):469-77 https://doi.org/10.1029/pa005i004p00469

Brown N, Galbraith ED (2016) Hosed vs. unhosed: interruptions of the Atlantic Meridional Overturning Circulation in a global coupled model, with and without freshwater forcing. Clim past 12:1663-79 https://doi.org/10.5194/cp-12-1663-2016

Calov R, Ganopolski A, Petoukhov V, Claussen M, Greve R (2002) Large-scale instabilities of the Laurentide ice sheet simulated in a fully coupled climate-system model. Geophys Res Lett 29(24):2216 https://doi.org/10.1029/2002GL016078

Carlson A (2008) Why there was not a Younger Dryas-like event during the Penultimate Deglaciation? Quat Sci Rev 27(9–10):882–7 https://doi.org/10.1016/j.quascirev.2008.02.004

Chappell J (2002) Sea level changes forced ice breakouts in the Last Glacial cycle: new results from coral terraces. Quat Sci Rev 21(10):1229–40 https://doi.org/10.1016/s0277-3791(01)00141-x

Charles CD, Lynch-Stieglitz J, Ninnemann US, Fairbanks RG (1996) Climate connections between the hemisphere revealed by deep sea sediment core/ice core correlations. Earth Planet Sci Lett 142(1-2):19-27 https://doi.org/10.1016/0012-821x(96)00083-0

Clark PU (1992) Surface form of the southern Laurentide Ice Sheet and its implications to ice sheet dynamics. Geol Soc Am Bull 104:595-605 https://doi.org/10.1130/0016-7606(1992)104<0595:sfotsl>2.3.co;2

Clark PU, Alley RB, Pollard D (1999) Northern Hemisphere ice sheet influences on global climate change. Science 286:1104–11 https://doi.org/10.1126/science.286.5442.1104

Crooks GE (1999) Entropy production fluctuation theorem and the nonequilibrium work relation for free energy differences. Phys Rev E 60(3):2721–6 https://doi.org/10.1103/physreve.60.2721

Dansgaard W, Johnsen SJ, Clausen HB, Dahl-Jensen D, Gundestrup NS, Hammer CU, Hvidberg CS, Steffensen JP, Sveinbjörnsdottir AE, Jouzel J, Bond G (1993) Evidence for general instability of past climate from a 250-kyr ice-core record. Nature 364(6434):218-20 https://doi.org/10.1038/364218a0

Denton GH, Alley RB, Comer GC, Broecker WS (2005) The role of seasonality in abrupt climate change. Quat Sci Rev 24(10-11):1159-82 https://doi.org/10.1016/j.quascirev.2004.12.002

de Vernal A, Eynaud F, Henry M, Hillaire-Marcel C, Londeix L, Mangin S, Matthiessen J, Mar-ret F, Radi T, Rochon A, Solignac S, Turon JL (2005) Reconstruction of sea surface conditions at middle to high latitudes of the Northern Hemisphere during the Last Glacial Maximum (LGM) based on dinoflagellate cyst assemblages. Quat Sci Rev (24):897–924 https://doi.org/10.1016/j.quascirev.2004.06.014

Duplessy JC, Labeyrie L, Arnold M, Paterne M, Duprat J, van Weering TC (1992) Changes in surface salinity of the North Atlantic Ocean during the last deglaciation. Nature 358(6386):485-8 https://doi.org/10.1038/358485a0

Elliot M, Labeyrie L, Duplessy JC (2002) Changes in North Atlantic deep-water formation associated with the Dansgaard–Oeschger temperature oscillations (60–10 ka). Quat Sci Rev 21(10):1153-65 https://doi.org/10.1016/s0277-3791(01)00137-8

Evans DJ, Searle DJ (2002) The fluctuation theorem. Adv Phys 51:1529 https://doi.org/10.1080/00018730210155133

Fairbanks RG (1989) A 17,000-year glacio-eustatic sea level record: Influence of glacial melting rates on the Younger Dryas event and deep-ocean circulation. Nature 342:637-42 https://doi.org/10.1038/342637a0

Fricker HA, Scambos T, Bindschadler R, Padman L (2007) An active subglacial water system in West Antarctica mapped from space. Science 315(5818):1544–8 https://doi.org/10.1126/ science.1136897

Ganopolski A, Rahmstorf S (2001) Rapid changes of glacial climate simulated in a coupled climate model. Nature 409:153-8

Grootes PM, Stuiver M (1997) Oxygen 18/16 variability in Greenland snow and ice with 103- to 105-year time resolution. J Geophys Res 102:26455-70 https://doi.org/10.1029/97jc00880

Grousset FE, Labeyrie L, Sinko JA, Cremer M, Bond G, Duprat J, Cortijo E, Huon S (1993) Patterns of ice-rafted detritus in the glacial North Atlantic (40–55° N). Paleoceanogr 8(2):175-92 https://doi.org/10.1029/92pa02923

Heinrich H (1988) Origin and consequences of cyclic ice rafting in the northeast Atlantic Ocean during the past 130,000 years. Quat Res 29:142-52 https://doi.org/10.1016/0033-5894(88)90057-9

Hemming SR (2004) Heinrich events: massive late Pleistocene detritus layers of the North Atlantic and their global climate imprint. Rev Geophys 42(1):RG1005,1-43 https://doi.org/10.1029/2003RG000128

Henry LG, McManus JF, Curry WB, Roberts NL, Piotrowski AM, Keigwin LD (2016) North Atlantic ocean circulation and abrupt climate change during the last glaciation. Science 353(6298):470-4 https://doi.org/10.1126/science.aaf5529

Hooke RL (1977) Basal temperatures in polar ice sheets: a qualitative review. Quat Res 7(1):1-13 https://doi.org/10.1016/0033-5894(77)90011-4

Keigwin LD, Jones GA, Lehman SJ, Boyle EA (1991) Deglacial meltwater discharge, North Atlantic deep circulation, and abrupt climate change. J Geophys Res Oceans 96(C9):16811-26 https://doi.org/10.1029/91jc01624

Kerr RA (2000) A North Atlantic climate pacemaker for the centuries. Science 288(5473):1984-5 https://doi.org/10.1126/science.288.5473.1984

Kleidon A (2009) Non-equilibrium thermodynamics and maximum entropy production in the Earth system: applications and implications. Naturwiss 96:653–77 https://doi.org/10.1007/s00114-009-0509-x

Kucera M, Weinelt M, Kiefer T, Pflaumann U, Hayes A, Weinelt M, Chen MT, Mix AC, Barrows TT, Cortijo E, Duprat J (2005) Reconstruction of sea-surface temperatures from assemblages of planktonic foraminifera: multi-technique approach based on geographically constrained calibration data sets and its application to glacial Atlantic and Pacific Oceans. Quat Sci Rev 24(7-9):951-98 https://doi.org/10.1016/j.quascirev.2004.07.014

Lehman SJ, Keigwin JD (1992) Sudden changes in North Atlantic circulation during the last deglaciation. Nature 356:757–62 https://doi.org/10.1038/356757a0

Li C, Battisti DS, Bitz CM (2010) Can North Atlantic sea ice anomalies account for Dansgaard–Oeschger climate signals? J Clim 23(20):5457-75 https://doi.org/10.1175/2010JCLI3409.1

Lozier MS (2010) Deconstructing the conveyer belt. Science 328(5985):1507-11 https://doi.org/10.1126/science.1189250

MacAyeal DR (1993) Binge/purge oscillations of the Laurentide ice sheet as a cause of the North Atlantic's Heinrich events. Paleoceanogr 8(6):775-84 https://doi.org/10.1029/93pa02200

Manabe S, Stouffer RJ (1988) Two stable equilibria of a coupled ocean-atmosphere model. J Clim 1:841-66 https://doi.org/10.1175/1520-0442(1988)001<0841:tseoac>2.0.co;2

Manabe S, Stouffer R (1999) The role of thermohaline circulation in climate. Tellus A 51(1):91-109 https://doi.org/10.1034/j.1600-0870.1999.t01-1-00008.x

Marchitto TM, Wei KY (1995) History of Laurentide meltwater flow to the Gulf of Mexico during the last deglaciation, as revealed by reworked calcareous nannofossils. Geology 23(9):779-82 https://doi.org/10.1130/0091-7613(1995)023<0779:holmft>2.3.co;2

Marotzke J, Stone P (1995) Atmospheric transports, the thermohaline circulation, and flux ad-justments in a simple coupled model. J Phys Oceanogr 25:1350-64 https://doi.org/10.1038/287430a0

McCabe AM, Clark PU (1998) Ice-sheet variability around the North Atlantic Ocean during the last deglaciation. Nature 392(6674):373-7 https://doi.org/10.1038/32866

McManus JF, Oppo DW, Cullen JL (1999) A 0.5-million-year record of millennial-scale climate variability in the North Atlantic. Science 283(5404):971-5 https://doi.org/10.1126/science.283.5404.971

Menviel L, Timmermann A, Friedrich T, England MH (2014) Hindcasting the continuum of Dansgaard-Oeschger variability: Mechanisms, patterns and timing. Clim Past 10:63-77 https://doi.org/10.5194/Cp-10-63-2014

Oerlemans J (1991) The mass balance of the Greenland ice sheet: sensitivity to climate change as revealed by energy-balance modelling. Holocene 1(1):40-8 https://doi.org/10.1177/095968369100100106

Ou HW (2001) Possible bounds on the earth's surface temperature: From the perspective of a conceptual global-mean model. J Clim 14:2976-88 https://doi.org/10.1175/1520-0442(2001)014<2976:pbotes>2.0.co;2

Ou HW (2018) Thermohaline circulation: a missing equation and its climate change implications. Clim Dyn 50:641-53 https://doi.org/10.1007/s00382-017-3632-y

Ou HW (2022) A theory of glacier dynamics and instabilities Part 1: Topographically confined glaciers. J Glaciol 68(267):1–12 https://doi.org/ 10.1017/jog.2021.20

Ozawa H, Ohmura A, Lorenz RD, Pujol T (2003) The second law of thermodynamics and the global climate system: A review of the maximum entropy production principle. Rev Geophys 41:4/10182003 https://doi.org/10.1029/2002rg000113

Paillard D (1995) The hierarchical structure of glacial climatic oscillations: Interactions between ice-sheet dynamics and climate. Clim Dyn 11:162–77 https://doi.org/10.1007/s003820050068

Rahmstorf S (2002) Ocean circulation and climate during the past 120,000 years. Nature 419:207–14 https://doi.org/10.1038/nature01090

Rahmstorf S, Crucifix M, Ganopolski A, Goosse M, Kamenkovich I, Knutti R, Lohmann G, Marsh R, Mysak LA, Wang Z, Weaver AJ (2005) Thermohaline circulation hysteresis: A model intercomparison. Geophys Res Lett 32(23) L23605, doi:10.1029/2005GL023655

Sakai K, Peltier WR (1999) A dynamical system model of the Dansgaard–Oeschger oscillations and the origin of the Bond cycle. J Clim 12:2238–55 https://doi.org/10.1175/1520-0442(1999)012<2238:adsmot>2.0.co;2

Schulz M, Paul A (2002) Holocene climate variability on centennial-to-millennial time scales: 1. Climate records from the North-Atlantic realm. In: Climate development and history of the North Atlantic realm (p 41-54). Springer, Berlin, Heidelberg.

Shakun JD, Clark PU, He F, Marcott SA, Mix AC, Liu Z, Otto-Bliesner B, Schmittner A, Bard E (2012) Global warming preceded by increasing carbon dioxide concentrations during the last deglaciation. Nature 484(7392):49-54 https://doi.org/10.1038/nature10915

Stocker TF (1998) The seesaw effect. Science 282(5386):61-2 https://doi.org/10.1126/science.282.5386.61

Stocker TF (2000) Past and future reorganization in the climate system. Quat Sci Rev 19:301-19 https://doi.org/10.1016/s0277-3791(99)00067-0

Stommel H (1961) Thermohaline convection with two stable regimes of flow. Tellus 13:224-30 https://doi.org/10.1111/j.2153-3490.1961.tb00079.x

Teller JT (1990) Meltwater and precipitation runoff to the North Atlantic, Arctic, and Gulf of Mexico from the Laurentide ice sheet and adjacent regions during the Younger Dryas. Paleoceanogr 5:897–905 https://doi.org/10.1029/pa005i006p00897

Tulaczyk S, Kamb WB, Engelhardt HF (2000) Basal mechanics of Ice Stream B, west Antarctica: 2. Undrained plastic bed model. J Geophys Res 105(B1):483–94 https://doi.org/10.1029/1999jb900328

Van Kreveld S, Sarnthein M, Erlenkeuser H, Grootes P, Jung S, Nadeau MJ, Pflaumann U, Voelker A (2000) Potential links between surging ice sheets, circulation changes, and the Dansgaard-Oeschger cycles in the Irminger Sea, 60–18 kyr. Paleoceanogr 15(4):425-42 https://doi.org/10.1029/1999pa000464

Wang GM, Sevick EM, Mittag E, Searles DJ, Evans DJ (2002) Experimental demonstration of violations of the Second Law of Thermodynamics for small systems and short time scales. Phys Rev Lett 89 (5):050601/1–050601/4 https://doi.org/10.1103/physrevlett.89.050601

Winton M, Sarachik ES (1993) Thermohaline oscillations induced by strong steady salinity forcing of ocean general circulation models. J Phys Oceanogr 23:1389-1410 https://doi.org/10.1175/1520-0485(1993)023<1389:toibss>2.0.co;2

Yokoyama Y, Esat TM (2011) Global climate and sea level: Enduring variability and rapid fluctuations over the past 150,000 years. Oceanogr 24(2):54-69 https://doi.org/10.5670/ oceanog.2011.27Alley RB (1998) Icing the north Atlantic. Nature 392(6674):335-7 https://doi.org/10.1038/32781